ACS SyntheticBiology

pubs.acs.org/synthbio Research Article

Two-Component Biosensors: Unveiling the Mechanisms of Predictable Tunability

Eva Gonzalez-Flo, Maria Elisenda Alaball, and Javier Macia*

Cite This: *ACS Synth. Biol.* 2020, 9, 1328–1335 Read Online

ABSTRACT: Many studies have been devoted to the engineering of cellular biosensors by exploiting intrinsic natural sensors. However, biosensors rely not only on input detection but also on an adequate response range. It is therefore often necessary to tune natural systems to meet the demands of specific applications in a predictable manner. In this study, we explored the customizability of two-component bacterial biosensors by modulating the main biosensor component, *i.e.*, the receptor protein. We developed a mathematical model that describes the functional relationship between receptor abundance and activation threshold, sensitivity, dynamic range, and operating range. The defined mathematical framework allows the design of the genetic architecture of a two-component biosensor that can perform as required with minimal genetic engineering. To experimentally validate the model and its predictions, a library of biosensors was constructed. The good agreement between theoretical designs and experimental results indicates that modulation of receptor protein abundance allows optimization of biosensor designs with minimal genetic engineering.

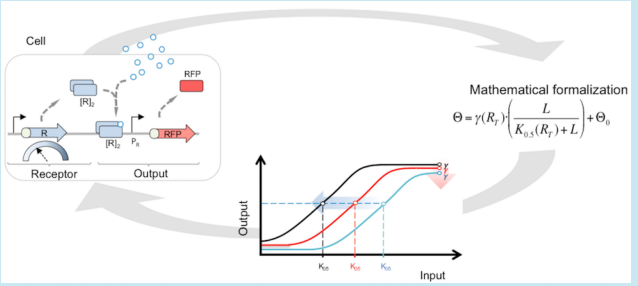

KEYWORDS: *biosensors, tunability, mathematical modeling*

The engineering of bacteria for the detection of biological signals has great potential in multiple fields such as biomedicine,[1] bioremediation,[2] and industry.[3] In this context, synthetic biology has emerged as a discipline in which modular biological parts can be used for the construction of cellular biosensors using a rational design, according to the principles of abstraction, standardization, and modularity.[4−6]

Based on the modularity principle, new biosensors can be assembled by combining different biological parts from different species in a host cell. In this way, intrinsic cellular machineries able to detect extracellular environments are exploited and rewired to create novel devices. However, in many cases the performance of such biosensors is not good enough to satisfy detection requirements.[7] There is therefore a need for the development of methodologies to modify biosensor features so that they can satisfy the demands of specific applications in a predictable way.

In the present study, we focused on the architecture of the two-component bacterial biosensors (TCBs), which are the most abundant biosensors in prokaryotic organisms and which act as major signal transduction devices for sensing and responding to different environmental conditions.[8] More specifically, TCB signal detection relies on the interaction between the two components that is mediated by the external signal. The first component of a TCB is a receptor protein that can bind an external signal and subsequently trigger the expression of the second TCB component, e.g., a fluorescent reporter protein. Although different methods for tuning biosensor responses have been explored,[9−12] the simplest strategy is based on modulation of the abundance of the first component, i.e., the receptor protein. The simplicity of this method, which allows specific modifications with minimal genetic manipulation, makes it suitable for designing synthetic bacterial sensors. Previous studies have reported that modulations in the receptor protein abundance either at transcriptional or post-transcriptional levels can be used to induce modifications in key biosensor parameters such as activation threshold, sensitivity, and dynamic range.[13−15] However, despite the experimental evidence, there is no formal theory that allows the design of customized biosensors in a systematic and predictable manner. To address this need, we developed a mathematical model that describes the functional relationship between the abundance of the receptor protein and the main features of a biosensor response. In detail, we identified the relationship between receptor protein abundance and the activation threshold, the dynamic range, the sensitivity, and the optimal operating range of the biosensor. It is worth mentioning that our model not only

Received: January 8, 2020
Published: May 5, 2020

https://dx.doi.org/10.1021/acssynbio.0c00010
ACS Synth. Biol. 2020, 9, 1328–1335

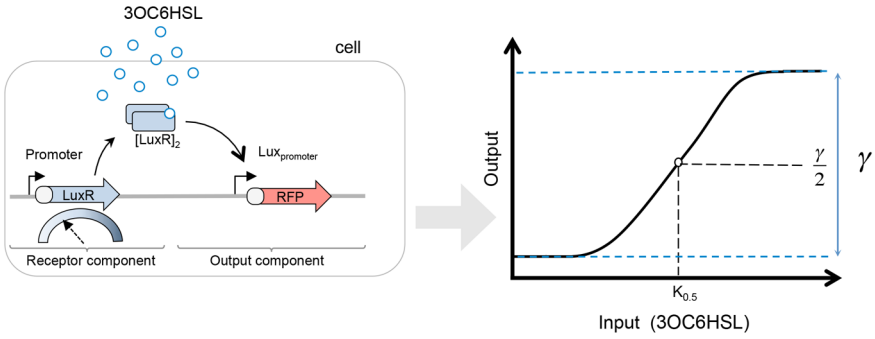

Figure 1. Schematic representation of two-component biosensor architecture. The first biosensor component (receptor component) is responsible for production of the receptor protein and consists of a terminator (BBa_B0014), a DNA promoter sequence (variable depending on the experimental setup), an RBS sequence (variable depending on the experimental setup), and the LuxR protein (BBa_C0062). The second biosensor component (output component) can respond in an inducible way to the complex of LuxR and 3OC6HSL due to the inducible lux promoter. The DNA cassette consists of a terminator (BBa_B0014), the Lux promoter (BBa_R0061), an RBS (BBa_B0034), and the output red fluorescent protein (RFP), (BBa_E1010). The transfer function, defined as the relationship between input and output, is characterized by $K_{0.5}$ and γ.

describes the functional dependence of these key parameters on receptor abundance but also allows prediction of the biosensor response for further configurations.

To experimentally validate the model and its predictions, a library of genetic devices that act as biosensors was constructed and used for proof-of-concept. Devices were designed based on the architecture of the well-known quorum sensing Lux system from *Vibrio fischeri*, which has been extensively used in synthetic biology.[16,17] In this system, the receptor protein, termed LuxR, is constitutively expressed, and in the presence of external molecules of 3-oxo-C6-homoserine lactone (3OC6HSL), the complex LuxR-3OC6HSL dimerizes and binds to the Lux promoter, thereby triggering the expression of a downstream gene, e.g., red fluorescent protein (RFP), that acts as a reporter.[18] Figure 1 shows a schematic representation of this system.

In conclusion, in this study we established a new mathematical formalization that allows the predictable design of biosensor systems in living cells and has further potential applications in many different fields of synthetic biology and biotechnology.

RESULTS AND DISCUSSION

Biosensor Mathematical Formalization Based on Two-Component Architecture. We developed an analytically tractable model that describes the dependence of the reporter gene expression at the steady state with respect to the relative abundance of the receptor protein (R_T) at different concentrations of external input (L) (see the Supporting Information for model details). As a result of our mathematical formalization, the relative expression of the reporter protein Θ produced upon an external input concentration L is described by

$$\Theta = \gamma(R_T)\left(\frac{L}{K_{0.5}(R_T) + L}\right) + \Theta_0 \tag{2}$$

Here, Θ_0 represents the basal expression of the reporter protein in the absence of inducer, i.e., $L = 0$; $\gamma(R_T)$ corresponds to the relative dynamic range, and $K_{0.5}(R_T)$ is the biosensor activation threshold, which is defined as the concentration of external input L that gives half-maximal response. Both terms depend on R_T, according to

$$\gamma(R_T) = \frac{b_1 \times R_T}{b_0 + b_1 \times R_T} \tag{3}$$

and

$$K_{0.5}(R_T) = \frac{a_1}{b_0 + b_1 \times R_T} \tag{4}$$

where a and b are model parameters determined as described in the next section.

Model Parameters Determination. To experimentally determine the model parameters a_1, b_0, and b_1, a library of biosensors that produce RFP in response to 3OC6HSL, based on the model described in Figure 1, was built. Each biosensor was designed to work at different LuxR concentrations by exploitation of constitutive promoters with variable strengths (constructs C1−C4 in Table S1).

In order to analyze biosensor response, the transfer function of each device, i.e., the relationship between input L (3OC6HSL) and output Θ (RFP), was measured (Figure S1), and γ and $K_{0.5}$ were experimentally determined. Values of γ were calculated by dividing RFP levels by the maximum RFP value, which corresponds to that obtained with construct C1 at the maximum induction level, i.e., $L = 10\ \mu$M. The dependence of γ and $K_{0.5}$ on the relative concentration of LuxR was determined. For this purpose, the relative LuxR concentrations were calculated by measuring the strengths of the different constitutive promoters upstream of LuxR in constructs C1−C4. To that end, a new set of genetic constructs (C8−C11 in Table S1), in which each constitutive promoter was individually located upstream of the reporter protein RFP, was built. Experimental measures of RFP levels allows to determine the relative activity of each promoter.[19] We used the strongest characterized promoter, i.e., the promoter J23100 in construct C8, as a reference to calculate the relative activity of each different promoter. Figure 2a shows the relative RFP expression levels. Finally, we assumed that the relative abundance of LuxR is proportional to the relative promoter activity located in upstream LuxR.[13] Figures 2b and 2c show the dependence of $K_{0.5}$ and γ, respectively, on the relative abundance of LuxR. Finally, eqs 3 and 4 were fitted to experimental values, and the model parameters a_1, b_0, and b_1 were determined. Matlab R2013a software was used for fitting the parameters. Parameter values obtained were $a_1 = 35\ \mu$M, $b_0 = 20$, and $b_1 = 2.6 \times 10.^3$ It is worth mentioning that, according

https://dx.doi.org/10.1021/acssynbio.0c00010
ACS Synth. Biol. 2020, 9, 1328−1335

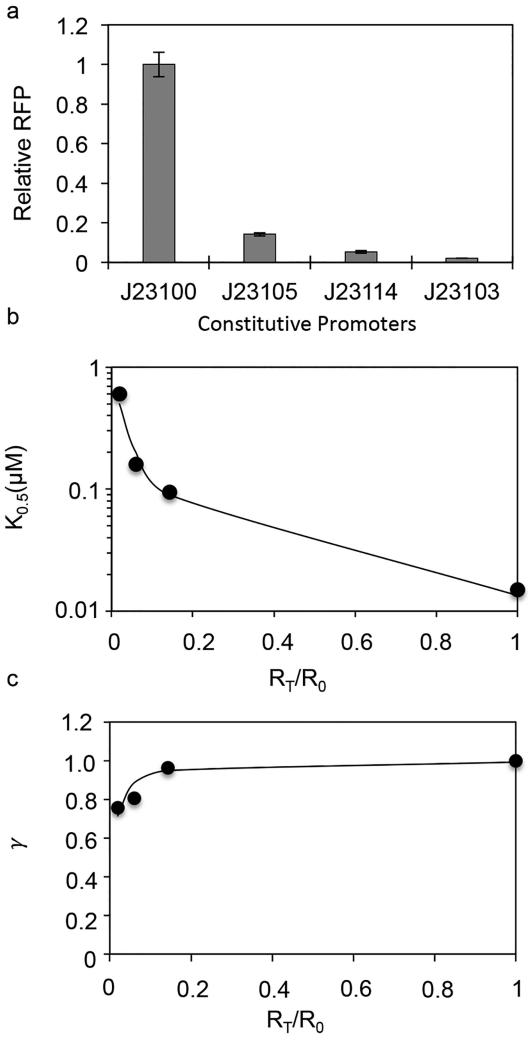

Figure 2. Model fitting. (a) Experimental characterization of RFP output from several constitutive promoters expressing different levels of LuxR (constructs C8−C11). RFP levels are indicated relative to those expressed from the J23100 promoter, which was assigned an arbitrary value of 1. (b) 3OC6HSL biosensor affinity ($K_{0.5}$) with respect to relative variations in LuxR expression levels. $K_{0.5}$ corresponds to the concentration of external input L that gives half-maximal response. The solid line corresponds to model eq 4 fitted to experimental values (dots) of $K_{0.5}$. (c) Relative dynamic range γ with respect to relative variations in LuxR expression levels. The solid line corresponds to model eq 3 fitted to experimental values (dots) of γ.

to the model equations, model parameters define all sets of biosensors based on the combination of receptor protein and its corresponding promoter regulating the output expression. Nonetheless, model parameters are independent of the mechanism regulating the receptor protein expression, i.e., either by a constitutive or inducible promoter.

Dependence of Sensitivity and Operating Range on Receptor Abundance. One of the most important features of a biosensor is the so-called sensitivity, σ. Biosensor sensitivity can be defined as the output variation for a given change in the input.[21] It should be mentioned that, for biosensors that display a nonlinear response, the value of σ is different for each input concentration L.

Our theoretical analyses and experimental data show that two-component biosensor transfer functions have three well-defined regions, with different sensitivities, as represented in Figure 3a. At low and high L concentrations (Regions I and III) the output Θ shows no significant dependence on the input, i.e., $\sigma \approx 0$. However, there is a significant increase in biosensor sensitivity within Region II that corresponds to the optimal biosensor operating range, i.e., the range of input concentrations that induce a significant change in the output.[22] For further mathematical analysis of this phenomenon, we defined parameter C as

$$C = \log(L) \tag{5}$$

Hence, eq 2 can be rewritten as

$$\Theta = \gamma\left(\frac{10^{C}}{K_{0.5}(R_T) + 10^{C}}\right) + \Theta_0 \tag{6}$$

With this reformulation, changes in L are parametrized by changes in C and the behavior of eq 6 presents a quasi-linear dependence with respect to C in Region II. As a consequence, sensitivity in this region can be approximated to

$$\sigma \approx \frac{d\Theta}{dC} \tag{7}$$

i.e.

$$\sigma \approx \frac{\gamma K_{0.5}(R_T) \times \ln(10)}{(K_{0.5}(R_T) + 10^{C})^2} \tag{8}$$

with $K_{0.5}(R_T)$ defined by eq 4. According to eq 8, a biosensor response has maximum sensitivity, i.e., $\frac{d\sigma}{dC} = 0$, at $C^* = \log(K_{0.5})$, which corresponds to $L = K_{0.5}$.

Here, we propose a mathematical definition of the Region II, i.e., the range of concentrations within which biosensor response exhibits higher sensitivity. This range can be determined by the upper and lower bonds, C^+ and C^-, that are defined by the intersection of the tangent to Θ at $C^* = \log(K_{0.5})$ with the maximum and minimum values of the transfer function, respectively. Figure 3a shows a representation of this geometrical definition. The tangent line can be described by using eq 6, and considering that at C^* the tangent line intersects the response curve at half-maximum amplitude, i.e., $f = \frac{\gamma}{2}$, we can write

$$f = \frac{\gamma \ln(10)}{4} \times C + \frac{\gamma}{2}[2 - \ln(10) \times \log(K_{0.5}(R_T))] \tag{9}$$

Finally, the range of input concentrations within which the biosensor has higher sensitivity can be defined by $f(C^-) = 0$ and $f(C^+) = \gamma$. By imposing these conditions, C^+ and C^- can be defined as

$$C^{\pm} = \frac{\log(K_{0.5}(R_T)) \times \ln(10) \pm 2}{\ln(10)} \tag{10}$$

Taking all of the above into consideration, the optimal operating range of the biosensor corresponds to the interval of input concentrations, in which the transfer function of the biosensor exhibits higher sensitivity. In this interval, the transfer function can be approximated to a linear dependence of Θ on $\log(L)$ described by

https://dx.doi.org/10.1021/acssynbio.0c00010
ACS Synth. Biol. 2020, 9, 1328−1335

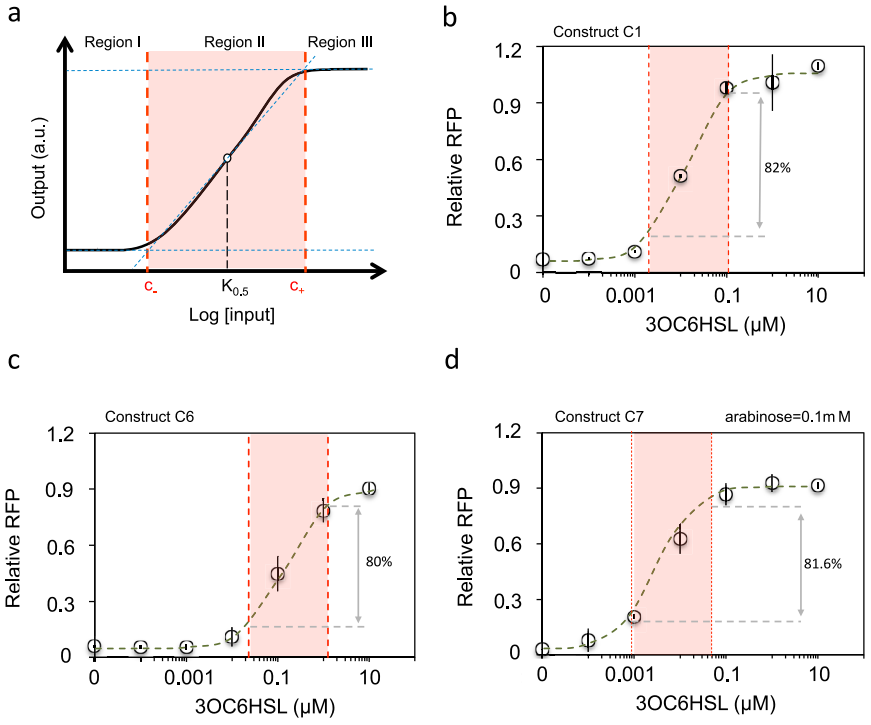

Figure 3. Mathematical determination of the biosensor operating range. (a) Schematic representation of the three different sensor regions determined. Dashed blue lines represent the geometrical method proposed to define the optimal operating range. (b–d) Several examples of the optimal operation range calculated according to eq 11. Dashed lines correspond to the Hill equation fitted to experimental data. Fitting parameters are shown in Table S3. In each figure, percentage corresponds to the total dynamic range within the theoretical operating range. The error bars shown in the figures are the standard deviation of four independent experiments.

$$\Theta \approx \frac{\gamma \ln(10)}{4} \times C + \frac{\gamma}{2}[2 - \ln(10) \times \log(K_{0.5}(R_T))] + \Theta_0 \quad (11)$$

In order to experimentally validate the defined operating range, given by eq 10, we applied this measurement to the whole set of biosensors described in Table S1 (constructs C1–C7). Figure 3b–d shows several examples of the theoretical calculation of the operating range, i.e., Region II superimposed on the experimentally obtained values. The remainder analyzed set of biosensors is shown in Figure S2. Our mathematical definition of the operating range captured at least 71.2% of the dynamic range of the biosensors operating region defined by eq 10. These data indicate that the operating range of two-component biosensors can be tuned by inducing the appropriate expression levels of the receptor protein R_T according to eq 10, independently of the method used to modify such receptor abundance.

Predictive Design of Two-Component Biosensors. The above-defined model describes the dependence of $K_{0.5}$ on the relative abundance of the receptor protein R_T, which enables the design of two-component biosensors with predefined $K_{0.5}$ values. $K_{0.5}$ defines both the activation threshold and the operating range of the sensor, i.e., the range of input concentrations within which the biosensor exhibits higher performance. Thus, two-component biosensors with predefined $K_{0.5}$ values can be designed in a straightforward manner by calculating the relative R_T levels necessary to build a genetic device with a given value of $K_{0.5}$, using the equation:

$$R_T(K_{0.5}) = \frac{a_1}{b_1 \times K_{0.5}} - \frac{b_0}{b_1} \quad (12)$$

To test the model predictability, we considered the implementation of several values of $K_{0.5}$. For each value we determined its corresponding relative R_T value using eq 12 and built a set of genetic constructs that produce the relative expression levels by the use of different architectures based on either constitutive (constructs C12–C13 in Table S1) or inducible (construct C14 in Table S1) promoters. The experimental characterization of these promoters is shown in Figure S3. It should be mentioned that the inducible system was implemented using the L-arabinose-dependent promoter pBad.[20] For the L-arabinose inducible system, the arabinose concentration required to implement a given $K_{0.5}$ was determined using a Hill function describing the relationship between promoter activity and arabinose concentrations (see Figure S3b). The relative promoter activity has been determined using eq 12.

Table 1 summarizes and compares the theoretical R_T values required to implement different $K_{0.5}$ values with those obtained experimentally using the constructs C12–C14.

Once the genetic systems producing the different relative levels of R_T were determined, a new set of biosensors based on the Lux system was built (constructs C5–C7 in Table S1). Using eqs 2–4, the transfer functions of the biosensors were theoretically predicted and compared with experimentally obtained results.

Figure 4a–e shows good agreement between the theoretically predicted and the experimentally obtained transfer functions. Figure S4 shows the experimental values of $K_{0.5}$ for the whole set of genetic constructs analyzed superimposed

https://dx.doi.org/10.1021/acssynbio.0c00010
ACS Synth. Biol. 2020, 9, 1328–1335

Table 1. Theoretical and Experimentally Obtained R_T Values Associated with $K_{0.5}$ Values

$K_{0.5}$ target	R_T levels (from eq 12)	genetic construct	experimental levels
4×10^{-1} μM	0.033	C5	0.026 ± 0.01
1.5×10^{-1} μM	0.11	C6	0.13 ± 0.02
6×10^{-2} μM	0.26	C7 + 10^{-3} mM arabinose	0.2 ± 0.08
10^{-2} μM	1.61	C7 + 10^{-2} mM arabinose	1.3 ± 0.1
5×10^{-3} μM	3.2	C7 + 10^{-1} mM arabinose	2.9 ± 0.35

on the theoretical curve described by eq 4. It should be mentioned that theoretical predictions accurately describe the experimental behavior independent of the features of the genetic system used to express LuxR at the required relative level. This fact indicates that abundance of the receptor protein R_T is the key regulatory factor, independently of the specific genetic system used to produce relative R_T abundance.

The design of genetic devices according to the fundamental principles of engineering is a big challenge in synthetic biology. It is necessary to develop tools and mathematical frameworks that will help to design and construct such devices in a predictable manner rather than by costly trial and error approaches.[23,24] Focusing on biosensor designs, many studies have been devoted to engineering new cellular devices by exploiting natural sensors present in cells.[25] However, biosensors have to work within an adequate operating range for the development of a specific application. It is therefore sometimes necessary to tune natural systems in terms of activation threshold, sensitivity, operating range, and dynamic range. In this study, we performed our analyses using one of the most abundant sensor systems in prokaryotes, the two-component sensor systems. We explored the possibility of adapting the two-component biosensor response by modulating the abundance of the main component, i.e., the receptor protein. To address this issue, we developed a mathematical model that determines the relationship between biosensor features and the abundance of receptor proteins. We further built a library of two-component biosensors based on the well-known Lux system.[17] As a first step, we analyzed only the effect of receptor abundance on $K_{0.5}$, and γ by introducing different constitutive promoters, with different strengths, upstream of the receptor protein. The experimental results, which were consistent with previously published data,[13,15] showed a clear correlation between threshold activation, parametrized by $K_{0.5}$, the relative dynamic range γ, and the sensitivity σ with LuxR relative concentrations. Experimental results were used to fit

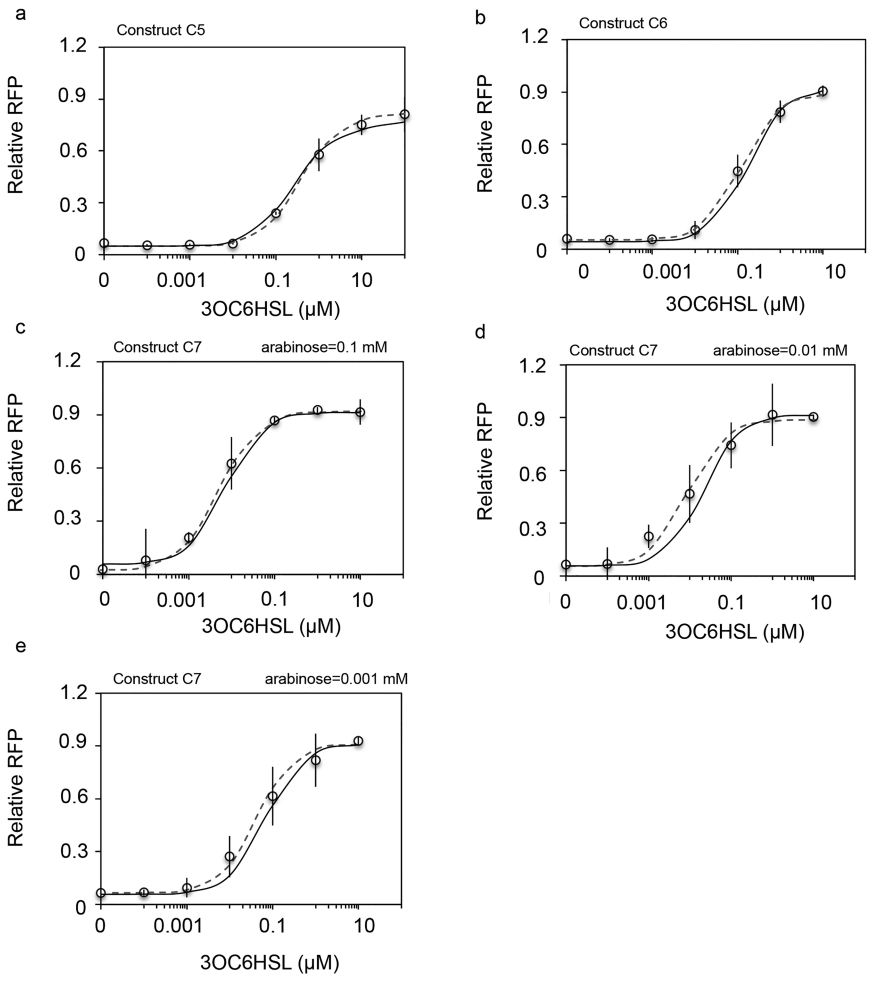

Figure 4. Model predictions of LuxR-dependent transfer functions. (a–e) Solid lines are the predicted transfer functions, dots are the experimentally determined values for the indicated constructs, and dashed lines are the Hill equation fitted to these experimental data. Fitting parameters are shown in Table S3. The error bars shown in the figures are the standard deviation of four independent experiments.

https://dx.doi.org/10.1021/acssynbio.0c00010
ACS Synth. Biol. 2020, 9, 1328–1335

the model and determine its parameters. Interestingly, once the parameters were determined, the mathematical model allowed prediction of the transfer function for a given abundance of receptor protein. In order to validate these predictions, we built several genetic systems in which LuxR relative levels could be modulated by changes in the promoter or the RBS, or by the addition of an extracellular effector. The relationship observed between $K_{0.5}$, representing the activation threshold of the biosensor, and the relative abundance of LuxR protein is remarkable. Notably, $K_{0.5}$ could be increased by up to 2 orders of magnitude by regulation of LuxR levels, independently of the method used to regulate receptor concentration. However, the dynamic range γ did not exhibit a strong dependence on LuxR abundance, meaning that transfer functions could be shifted toward greater or lower values of 3OC6HSL without a major impact on the dynamic range.

It is worth mentioning that the model derivation assumes that the abundance of receptor protein is large enough to consider a linear relationship between the concentrations of monomeric and dimeric forms of the receptor protein. This assumption can limit the applicability of the model to those situations in which receptor protein concentrations are very low. However, experimental results demonstrated that even for promoters with very low activities (construct C11 in Figure S3a) the theoretical calculations properly describe the experimental data, suggesting that the model is of general applicability for a broad range of genetic architectures.

Particularly notable were the results of the analysis of biosensor sensitivity. Due to the nonlinear response of the genetic systems, it is not possible to determine a single numerical value for their sensitivity. Despite showing a different sensitivity at each input concentration it was possible to distinguish two regions of low sensitivity, i.e., one at low- and one at high-input concentrations, and a high sensitivity region at intermediate-input concentrations. Interestingly, the intermediate-input concentration region determines the input ranges that induce the maximal output variation, which corresponds to the optimal operating range of the biosensor. We have proposed a new method that allows theoretical calculation of such a range of input concentrations. Furthermore, our model allows calculation of the abundance of receptor protein necessary to adjust this optimal operating range to a given input range. Experimental results show good agreement with our theoretical predictions, thus validating our model.

Future work should be devoted to exploring the feasibility of using the current developed model for predictable biosensor designs in other systems based on similar two-component architecture. Recent studies have demonstrated the application of synthetic biology biosensors in environmental monitoring,[26,27] bioproduction,[28,29] biomedical applications in diagnostics,[30] and health monitoring.[31] However, an ability to detect relevant inputs is not sufficient for the construction of commercial cell-based biosensors. Relevant input detection should be coupled with output detection within the appropriate range of input concentrations for each specific application. We aimed to overcome the above limitations by developing a theoretical and experimental framework that explains the relationships between the main features of biosensor components.

METHODS

Strains, Media, and Growth Conditions. Cloning and expression experiments were performed in *Escherichia coli* Top10 (Invitrogen, USA). Cells were grown in lysogeny broth (LB) at 37 °C and selected with the appropriate antibiotics (chloramphenicol 35 μg/mL, kanamycin 35 μg/mL; Sigma, USA). Bacterial strains were preserved in LB glycerol 20% (v/v) at −80 °C. Single colonies obtained from streaked glycerol stocks were inoculated, and the cells were grown overnight at 37 °C with shaking (200 rpm). Overnight cultures were diluted into fresh LB (1/100 dilution) and grown for 5 h. Diluted cultures were loaded into a 96-well microplate (Nunc, Thermo Fisher Scientific, USA) and induced (see below) in a final volume of 200 μL.

Genetic Sensors. Construction of the genetic sensors by cloning was carried out using the Biobrick assembly method and parts from the Spring 2018 iGEM distribution (http://parts.igem.org). All the constructs analyzed in this paper were built by combining these parts using a 3A assembly. Table S1 shows the genetic structures of the different constructs. Biobrick cloning was performed using an assembly kit (Ginkgo Bioworks, USA). All constructs were included in the Biobricks high copy number plasmid (pSB1AK3) and were transformed using a chemical method. Sanger sequencing confirmed all genetic constructs. Table S2 contains the sequences of all genetic parts used, and plasmid maps of genetic constructs are available in the Supporting Information.

Fluorescence Assays for Gene Expression Determination. Colonies of strains containing the plasmid of interest that were obtained from streaked glycerol stocks were grown overnight in LB kanamycin at 37 °C with continuous shaking. A 100-fold dilution of the overnight culture was grown in fresh LB kanamycin media until the exponential phase, OD660 ≈ 0.4, was reached. Induction media consisted of LB kanamycin and the appropriate inducer or inducer combination, i.e., 3OC6HSL (*N*-[-ketocaproyl]-L-homoserine lactone; Cayman Chemical Company, USA) and arabinose (L-(+)-arabinose 98%; Sigma Aldrich, USA). Different 3OC6HSL concentrations were prepared from an initial stock of 4×10^{-2} M. Serial dilutions in LB kanamycin, providing final concentrations ranging from 10 μM to 0.001 μM, were prepared the day of the experiment. Different arabinose concentrations were prepared from an initial stock of 0,74 M. Serial dilutions in LB kanamycin, providing final concentrations ranging from 0.1 mM to 0.001 mM, were prepared the day of the experiment.

Incubation for *in vivo* measurements was carried out by transferring 2 μL of the diluted cultures and 200 μL of LB kan0061mycin induction media into a flat bottomed 96-well microplate. LB without cells was also incubated as a background control for both fluorescence and absorbance. Figure S5 shows the resulting growth curves.

Gene expression induced by a wide range of 3OC6HSL and arabinose concentrations over time was monitored by quantification of the RFP. The bacterial cultures were incubated and induced on a Synergy MX microplate reader (BioTek Instruments, USA), and measurements were taken every 30 min for 20 h. Conditions for fluorescence measurements of the red fluorescent protein (RFP) were excitation at 578 ± 9 nm and emission at 616 ± 9 nm, with a gain of 50.

Sample (S) absorbance and fluorescence (f) readings (OD660(S) and $f(S)$, respectively) were corrected using respective signal background (B) controls (OD660(B), $f(B)$).

https://dx.doi.org/10.1021/acssynbio.0c00010
ACS Synth. Biol. 2020, 9, 1328−1335

Averaged data were obtained from three independent experiments. Reporter protein Θ was calculated according to the expression:

$$\Theta = \frac{f(S) - f(B)}{OD_{660}(S) - OD_{660}(B)} \quad (13)$$

The value Θ corresponds, with a factor of proportionality, to the concentration of the RFP protein per cell.

■ ASSOCIATED CONTENT

Supporting Information

The Supporting Information is available free of charge at https://pubs.acs.org/doi/10.1021/acssynbio.0c00010.

Tables with the plasmids and strains used in the study, mathematical model and parameters for model fitting, as well as supplementary figures that support the results shown in the main text (PDF)

■ AUTHOR INFORMATION

Corresponding Author

Javier Macia − *Synthetic Biology for Biomedical Applications Group, Department of Experimental and Health Sciences, Universitat Pompeu Fabra (UPF), E-08003 Barcelona, Spain;* orcid.org/0000-0002-6705-5554; Email: javier.macia@upf.edu

Authors

Eva Gonzalez-Flo − *Synthetic Biology for Biomedical Applications Group, Department of Experimental and Health Sciences, Universitat Pompeu Fabra (UPF), E-08003 Barcelona, Spain;* orcid.org/0000-0001-6560-9018

Maria Elisenda Alaball − *Synthetic Biology for Biomedical Applications Group, Department of Experimental and Health Sciences, Universitat Pompeu Fabra (UPF), E-08003 Barcelona, Spain; Imperial College London, Gradpad Wood Lane, London SW7 2AZ, U.K.;* orcid.org/0000-0002-1868-2674

Complete contact information is available at: https://pubs.acs.org/10.1021/acssynbio.0c00010

Author Contributions

E.G.F. and J.M. conceived the experimental design, interpreted the results, and wrote the manuscript. M.E.A. and E.G.F. performed the experiments. J.M. developed the mathematical model.

Funding

The authors are thankful for funding for the open access charge from the Spanish Ministry of Economy and Competitiveness [MINECO AEI-FIS2017-88786-R and FEDER] and UPF Valora Horitzó 2025 with the support of the Secretariat of Universities and Research of the Department of Business and Knowledge of the Generalitat de Catalunya and the co-financing of the European Regional Development Fund (FEDER). E.G.F. is a recipient of an FI-DGR (2017 FI_B 00018) fellowship.

Notes

The authors declare no competing financial interest.

■ ACKNOWLEDGMENTS

We thank all the members of the Synthetic Biology for Biomedical Applications Lab for fruitful conversations and the "Unidad de Excelencia María de Maeztu", funded by the AEI (CEX2018-000792-M).

■ REFERENCES

(1) Pan, Y., Hu, N., Wei, X., Gong, L., Zhang, B., Wan, H., and Wang, P. (2019) 3D cell-based biosensor for cell viability and drug assessment by 3D electric cell/matrigel-substrate impedance sensing. *Biosens. Bioelectron. 130*, 344−51.

(2) Wan, X., Volpetti, F., Petrova, E., French, C., Maerkl, S. J., and Wang, B. (2019) Cascaded amplifying circuits enable ultrasensitive cellular sensors for toxic metals. *Nat. Chem. Biol. 15*, 540−548.

(3) Khalil, A. S., and Collins, J. J. (2010) Memory elements Synthetic biology: applications come of age. *Nat. Rev. Genet. 11* (5), 367−79.

(4) Andrianantoandro, E., Basu, S., Karig, D. K., and Weiss, R. (2006) Synthetic biology: New engineering rules for an emerging discipline. *Mol. Syst. Biol. 2*, 1−14.

(5) Endy, D. (2005) Foundations for engineering biology. *Nature 438*, 449−453.

(6) Brophy, J., and Voigt, C. A. (2014) Principles of genetic circuit design. *Nat. Methods 11* (5), 508−20.

(7) Van Der Meer, J. R., Tropel, D., and Jaspers, M. (2004) Illuminating the detection chain of bacterial bioreporters. *Environ. Microbiol. 6* (10), 1005−20.

(8) Stock, A. M., Robinson, V. L., and Goudreau, P. N. (2000) Two-Component Signal Transduction. *Annu. Rev. Biochem. 69* (1), 183−215.

(9) French, C. E., de Mora, K., Joshi, N., Elfick, A., Haseloff, J., and Ajioka, J. (2011) Synthetic biology and the art of biosensor design. *The Science and Applications of Synthetic and Systems Biology*; National Academies Press: Washington DC, USA.

(10) Chen, Y., Ho, J. M. L., Shis, D. L., Gupta, C., Long, J., Wagner, D. S., Ott, W., Josic, K., and Bennett, M. R. (2018) Tuning the dynamic range of bacterial promoters regulated by ligand-inducible transcription factors. *Nat. Commun. 9*, 64.

(11) Shopera, T., Henson, W. R., Ng, A., Lee, Y. J., Ng, K., and Moon, T. S. (2015) Robust, tunable genetic memory from protein sequestration combined with positive feedback. *Nucleic Acids Res. 43* (18), 9086−94.

(12) Lu, M. S., Mauser, J. F., and Prehoda, K. E. (2012) Ultrasensitive synthetic protein regulatory networks using mixed decoys. *ACS Synth. Biol. 1* (2), 65−72.

(13) Wang, B., Barahona, M., and Buck, M. (2015) Amplification of small molecule-inducible gene expression via tuning of intracellular receptor densities. *Nucleic Acids Res. 43* (3), 1955−64.

(14) Carbonell-Ballestero, M., Duran-Nebreda, S., Montañez, R., Solé, R., Macía, J., and Rodríguez-Caso, C. (2014) A bottom-up characterization of transfer functions for synthetic biology designs: Lessons from enzymology. *Nucleic Acids Res. 42* (22), 14060−9.

(15) Ang, J., Harris, E., Hussey, B. J., Kil, R., and McMillen, D. R. (2013) Tuning response curves for synthetic biology. *ACS Synth. Biol. 2* (10), 547−67.

(16) Garcia-Ojalvo, J., Elowitz, M. B., and Strogatz, S. H. (2004) Modeling a synthetic multicellular clock: Repressilators coupled by quorum sensing. *Proc. Natl. Acad. Sci. U. S. A. 101* (30), 10955−60.

(17) Williams, J. W., Cui, X., Levchenko, A., and Stevens, A. M. (2008) Robust and sensitive control of a quorum-sensing circuit by two interlocked feedback loops. *Mol. Syst. Biol. 4*, 234−45.

(18) Fuqua, W. C., Winans, S. C., and Greenberg, P. E. (1994) Quorum Sensing in Bacteria: the LuxR-LuxI Family of Cell Density-Responsive Transcriptional Regulators. *J. Bacteriol. 176* (2), 269−275.

(19) Kelly, J. R., Rubin, A. J., Davis, J. H., Ajo-Franklin, C. M., Cumbers, J., Czar, M. J., de Mora, K., Glieberman, A. L., Monie, D. D., and Endy, D. (2009) Measuring the activity of BioBrick promoters using an in vivo reference standard. *J. Biol. Eng. 3*, 4.

(20) Khlebnikov, A., Risa, O., Skaug, T., Carrier, T. A., and Keasling, J. D. (2000) Regulatable arabinose-inducible gene expression system with consistent control in all cells of a culture. *J. Bacteriol. 182* (24), 7029−34.

(21) Banica, F. G. (2012) *Chemical Sensors and Biosensors: Fundamentals and Applications*; John Wiley & Sons: Chichester, U.K.
(22) Hicks, M., Bachmann, T. T., and Wang, B. (2020) Synthetic Biology enables programmable cell-based biosensors. *ChemPhysChem 21*, 132.
(23) Kwok, R. (2010) Five hard truths for synthetic biology. *Nature 463* (7279), 288−90.
(24) Lucks, J. B., Qi, L., Whitaker, W. R., and Arkin, A. P. (2008) Toward scalable parts families for predictable design of biological circuits. *Curr. Opin. Microbiol. 11* (6), 567−73.
(25) Carpenter, A. C., Paulsen, I. T., and Williams, T. C. (2018) Blueprints for biosensors: Design, limitations, and applications. *Genes 9* (8), 375.
(26) Chang, H. J., Voyvodic, P. L., Zúñiga, A., and Bonnet, J. (2017) Microbially derived biosensors for diagnosis, monitoring and epidemiology. *Microb. Biotechnol. 10* (5), 1031−5.
(27) *Biosensors for Environmental Monitoring*; Rinken, T., and Kivirand, K., Eds.; IntechOpen: 2019.
(28) Rogers, J. K., and Church, G. M. (2016) Genetically encoded sensors enable real-time observation of metabolite production. *Proc. Natl. Acad. Sci. U. S. A. 113* (9), 2388−93.
(29) Pandi, A., Grigoras, I., Borkowski, O., and Faulon, J. L. (2019) Optimizing Cell-Free Biosensors to Monitor Enzymatic Production. *ACS Synth. Biol. 8* (8), 1952−7.
(30) Zhou, W., Jimmy Huang, P. J., Ding, J., and Liu, J. (2014) Aptamer-based biosensors for biomedical diagnostics. *Analyst 139* (11), 2627−40.
(31) Mimee, M., Nadeau, P., Hayward, A., Carim, S., Flanagan, S., Jerger, L., Collins, J., McDonnell, S., Swartwout, R., Citorik, R. J., Bulović, V., Langer, R., Traverso, G., Chandrakasan, A. P., and Lu, T. K. (2018) An ingestible bacterial-electronic system to monitor gastrointestinal Health. *Science 360* (6391), 915−918.

https://dx.doi.org/10.1021/acssynbio.0c00010
ACS Synth. Biol. 2020, 9, 1328−1335